



Jones, K.A., Paterson, C.A., Hamilton, D.J., Small, A.D., Martin, W., Robinson, J. and Goodfield, N.E.R. (2021) Optimising approximate entropy for assessing cardiac dyssynchrony with radionuclide ventriculography. *Biomedical Signal Processing and Control*, 68, 102703.

(doi: [10.1016/j.bspc.2021.102703](https://doi.org/10.1016/j.bspc.2021.102703))

This is the Author Accepted Manuscript.

There may be differences between this version and the published version. You are advised to consult the publisher's version if you wish to cite from it.

<https://eprints.gla.ac.uk/240971/>

Deposited on: 10 May 2021

# Optimising approximate entropy for assessing cardiac dyssynchrony with radionuclide ventriculography

K.A. Jones<sup>1,2</sup>, C.A. Paterson<sup>1,2</sup>, D.J. Hamilton<sup>2</sup>, A.D. Small<sup>1,3</sup>,  
W. Martin<sup>1,2</sup>, J. Robinson<sup>1,2</sup> N.E.R. Goodfield<sup>1</sup>

<sup>1</sup>Department of Nuclear Cardiology, Glasgow Royal Infirmary, UK

<sup>2</sup>School of Physics and Astronomy, University of Glasgow, UK

<sup>3</sup>School of Medicine, Dentistry and Nursing, University of Glasgow, UK

E-mail: k.jones.3@research.gla.ac.uk

Left ventricular dyssynchrony can be assessed with phase parameters from radionuclide ventriculography (RNVG), including approximate entropy (*ApEn*). The input values used to calculate *ApEn* will affect the results significantly, so it is essential to optimise *ApEn* for the application. However to date, no optimisation for *ApEn* applied to images has been published. In this paper, generated data were used to simulate patient phase images, allowing the input parameters for *ApEn* to be tested and optimised in a controlled environment. Clinical images were then used to confirm that the selected parameters were appropriate. The results demonstrate the effect of input parameters for *ApEn* and the most appropriate use with RNVG phase images. This work demonstrates the importance of optimisation and standardisation when using *ApEn* as a measure of dyssynchrony.

*Keywords:* Approximate entropy, RNVG phase, Cardiac dyssynchrony

## 1. Introduction

Measures of left ventricular cardiac function provide important clinical information relating to diagnosis, treatment, and patient outcome [1–3]. Radionuclide ventriculography (RNVG) is an established cardiac imaging technique used to measure left ventricular ejection fraction (LVEF) and assess ventricular wall motion.

LVEF is a measure, expressed as a percentage, of how much blood is pumped by the left ventricle during each contraction and is known to be a powerful prognostic indicator of cardiovascular disease. It is a predictor of morbidity and mortality after a myocardial infarction (MI), and a low LVEF can indicate heart failure. Recently, there has been increased interest in using cardiac imaging to assess the mechanical dyssynchrony of the left ventricle. Left ventricular dyssynchrony can be quantified using several different phase parameters, including the standard deviation of the phase pixel values (phase

$SD$ ) and the bandwidth of the phase histogram. Approximate entropy ( $ApEn$ ) has been applied to phase images to quantify dyssynchrony [4, 5], but to date no optimisation for this application has been published. The selection of input values used will significantly affect the value of  $ApEn$ , therefore, this work aims to optimise  $ApEn$  for application to nuclear cardiology images and demonstrate the effect of changing input parameters.

### 1.1. RNVG phase images

An RNVG scan is performed by labelling the patient’s red blood cells with Technetium-99m Pertechnetate, allowing the changing volume of blood within the ventricles to be imaged from the resultant gamma emissions.

A phase image can be created from gated RNVG data to assess ventricular dyssynchrony [6, 7], using the time-activity curve from the first-order Fourier analysis for each pixel in the RNVG image. The resulting phase image represents the timing of contraction, relative to the R-R interval of the ECG. In a phase image for a patient with normal ventricular contraction, the pixels within the ventricles will all have a similar phase value, representing synchronous contraction. Regions of dyssynchronous contraction will have a higher phase value indicating delayed contraction as illustrated in Figure 1, where the phase for a patient who has had an MI has a distinctly different phase pattern compared to the patient with normal contraction. The time-activity curve for each example shows the average change in counts in the left ventricle (LV) over the average cardiac cycle. Comparing the normal and MI curves, the MI patient has noticeably slower filling. Other conduction abnormalities such as left bundle branch block (LBBB), a conduction delay that affects the timing of contraction, also have a distinct phase pattern. Dyssynchronous cardiac contraction can severely reduce the efficiency of the heart and worsen the clinical outcome for the patient.

### 1.2. Approximate entropy

Various cardiac dyssynchrony parameters have been established. However, most are derived from the first-order statistics, such as the mean and phase  $SD$ .

*Synchrony* and *entropy* were derived by O’Connell et al. as measures of cardiac dyssynchrony. *Synchrony* describes the contraction of the left ventricle using the phase and amplitude data extracted from the region defining the LV, and *entropy* (from Shannon information theory, [8]), is a measure of randomness within the ventricle [9]. They demonstrated that for discriminating between a normal and abnormal contraction, *synchrony* and *entropy* were superior to the phase  $SD$ .

However, the parameters previously investigated (mean, phase  $SD$ , *synchrony* and *entropy*) do not take into account the spatial relation between the phase values. More advanced statistical parameters, such as  $ApEn$ , can also be used to assess ventricular phase quantitatively.  $ApEn$  is a regularity statistic developed from Kolmogorov-Sinai entropy by Pincus [8], which calculates the probability that a series of length  $m$  remains

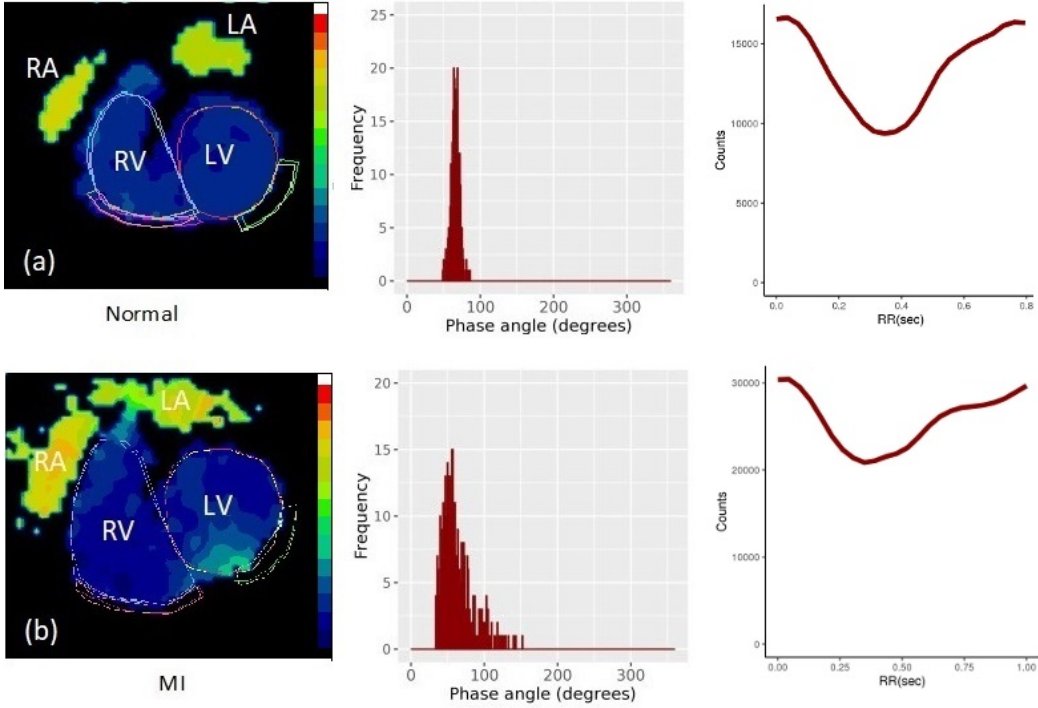


**Figure 1.** Example showing the phase pattern, LV phase histogram and associated time-activity curve for (a) a patient with normal LV function with similar phase values throughout the ventricles, (b) a patient who has an MI, resulting in late phase values in the area of the MI. In the phase image, the left and right ventricles (LV and RV) have a region of interest drawn around them. The pixel values within the LV are plotted in the associated phase histogram. The left and right atria (LA and RA) can also be seen in the phase image; the different colour represents the difference in timing between the ventricles and atria.

within a tolerance  $r$  at the next sequence in the data series. Unlike *entropy*,  $ApEn$  takes into account the similarity of adjacent data points.

$ApEn$  is used in other fields including heart rate variability and gait analysis [9–16], but has not been widely investigated for assessing images.

$ApEn$  was used for serial assessment of RNVG images for a small study of breast cancer patients, where a significant change in ejection fraction and  $ApEn$  was demonstrated over the course of treatment. Recent work carried out by our group demonstrated the predictive value of  $ApEn$  combined with LVEF for baseline assessment of breast cancer patients, before undergoing cardiotoxic chemotherapy [5].

$ApEn$  is defined as

$$ApEn = -(N - m)^{-1} \sum_{i=1}^{N-m} \ln \left( \frac{C_{i^{m+1}}(r)}{C_{i^m}} \right) \quad (1)$$

where  $N$  is the length of data series,  $m$  is the sequence length, and  $r$  is the tolerance.  $C_{i^m}(r)$  is the conditional probability that when a sequence is within the tolerance, the

next element will also be within tolerance. For this application, the pixel values are considered as a data series. Each sequence of ' $m$ ' pixels will be compared to every other sequence of ' $m$ ' pixels within the region of interest, including itself. If it is within the tolerance value  $r$ , it will be counted. This is repeated for every sequence of ' $m$ ' pixels then carried out using a new sequence of ' $m+1$ ' to calculate  $C_{i^m}$  and  $C_{i^{m+1}}$ . For example, if  $m = 2$  then each sequence of 2 pixels will be compared to every other sequence of 2 pixels within the data. The comparison would then be repeated for a sequence of ' $m + 1$ '. In this example, this would mean a sequence of 3 pixels would be then be compared.

*ApEn* includes a 'self match' when calculating  $C_{i^m}$ , creating a bias towards regularity. Published data suggest that *ApEn* lacks relative consistency, resulting in the value of *ApEn* 'flipping' when the input parameters are changed [17, 18]. For example, when using a low value of  $r$ , *ApEn* for a normal data series would be higher than for an abnormal data series. However, using a higher value of  $r$ , this would be the other way around. For this reason, sequence length  $m$  and tolerance  $r$  should be fixed when comparing data sets. There is currently no established  $m$ ,  $r$  or normal range for *ApEn* applied to phase images. The selection of  $m$  and  $r$  will markedly affect *ApEn*, so it is essential to optimise the input parameters for the data being considered [18–20].

## 2. Method

### 2.1. Generated data

All data analysis and statistics were performed in R 3.6.3 (R Development Core Team, Vienna, Austria) [21]. In order to gain full control of the input data a Monte Carlo generator based on a simple repeated random number sampling algorithm was developed. Image pixels in a chosen region of interest were divided into sixteen radial segments, with the phase value for each pixel assigned randomly according to a user-defined probability distribution function for each segment. This was implemented with Gaussian probability distribution functions for which the user would define the mean and *SD*. The region of interest size and pixel values of the simulated data were based on clinical data. Pixels outside of the LV region of interest were set to zero and excluded from the *ApEn* calculation. Simulated normal and MI phase images were created to investigate the effect of the input parameters.

### 2.2. Selecting $m$ and $r$

*ApEn* was calculated for varying values of sequence length  $m$  and tolerance  $r$  to demonstrate the effect of these input parameters. Some publications suggest using a value of  $r$  between 0.1 - 0.2 of the standard deviation of the dataset [8, 22]. However, for improved consistency, it is better to use a constant value of  $r$  [19]. For the groups of patient data used, the average *SD* of the phase pixel values was 8.1 for the normal group, and 18.2 for the MI group. 0.1 - 0.2 times the standard deviation for this data would suggest a range of  $r$  between 0.81 and 3.64, which was initially used as a starting

point. The final range tested was  $m$  between 1 and 5, with  $r$  from 0.25 extending until  $ApEn$  approached zero for a normal phase image. The majority of published papers use  $m = 2$ , although there is limited justification for this choice in the literature.

The initial optimisation was carried out using simulated images representing a normal and MI phase pattern. This was then repeated using clinical images for normal (187 patients), MI (164 patients) and LBBB (112 patients). The patient groups were defined by their clinical diagnosis, so some of MI patients may still have normal, or close to normal, LV function with a normal phase image.

### 2.3. Effect of data length

Left and right ventricular volumes vary from patient to patient, and subsequently, the number of pixels in the region of interest for each ventricle also varies. Simulated data were used to investigate the relation between  $ApEn$  and LV size. Simulated data as described in Section 2.1 was created with a radius varying from 7 to 15 pixels to cover the clinically significant range.  $ApEn$  was calculated for each LV size, to ensure that any difference between patients would be independent of LV size.

### 2.4. Data Order

First-order measures such as *synchrony* and *entropy* have no dependence on data order. However, for  $ApEn$ , the order is important. The algorithm reads the phase image and converts it into a matrix, with each pixel representing the phase value. The matrix is then converted into a one-dimensional data series for the  $ApEn$  calculation. The direction that the matrix is read in will change the order of the pixel values used in the  $ApEn$  calculation.  $ApEn$  is usually applied to time series data, where the order is set, so to investigate the effect of reading the matrix in different directions, the code was modified to read the data in different orders to allow comparison. The  $m$  and  $r$  values used for the testing data order were selected based on the optimisation work.

The diagram in Figure 2 illustrates the four different directions that the image data were read. In Figure 2 (a), the data is read from left to right, but this means that in a group of  $m$  pixels, they may not be adjacent to each other in the image even though they are adjacent in the data series. One pixel could be from the lateral wall of the LV, and the next pixel would be from the septum at the start of the next line. This is unlikely to make a difference in a normal phase image where all the pixels have a similar value but could have an impact when investigating a patient with a more abnormal phase image. The group tested consisted of 187 normal and 164 MI patients. Receiver operator characteristic (*ROC*) analysis was used to determine if the data order affected the ability to discriminate between normal and MI patients. The mean  $\pm$  *SD*, area under the curve (*AUC*) with 95% confidence intervals (*CI*) were calculated for each data order.

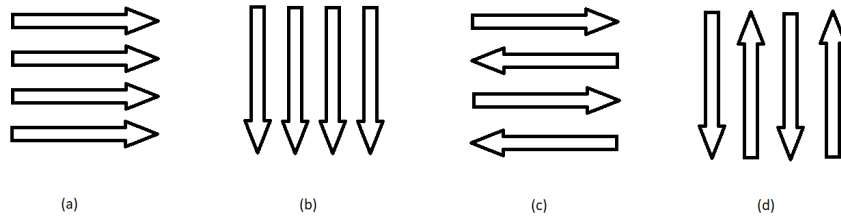


**Figure 2.** The four directions tested for reading the image matrix, reading image from (a) left to right, (b) top to bottom, (c) left - right, right - left etc (d) top - bottom, bottom to top etc.

### 3. Results and discussion

#### 3.1. Final selection of sequence length ( $m$ )

The variation of  $ApEn$  with sequence length  $m$  and tolerance  $r$  is shown in Figure 3. At higher values of  $m$ , there will be fewer matches, and  $ApEn$  decreases towards zero, meaning there would not be sufficient separation to distinguish between normal and abnormal phase images. This data illustrates the importance of optimising  $m$  and  $r$  and suggests that a value of  $m$  equal to 1 or 2 would be most appropriate. However, a value of 1 would result in a reduced dependence on the spatial relation of each pixel. For this reason, a sequence length of  $m = 2$  was chosen.

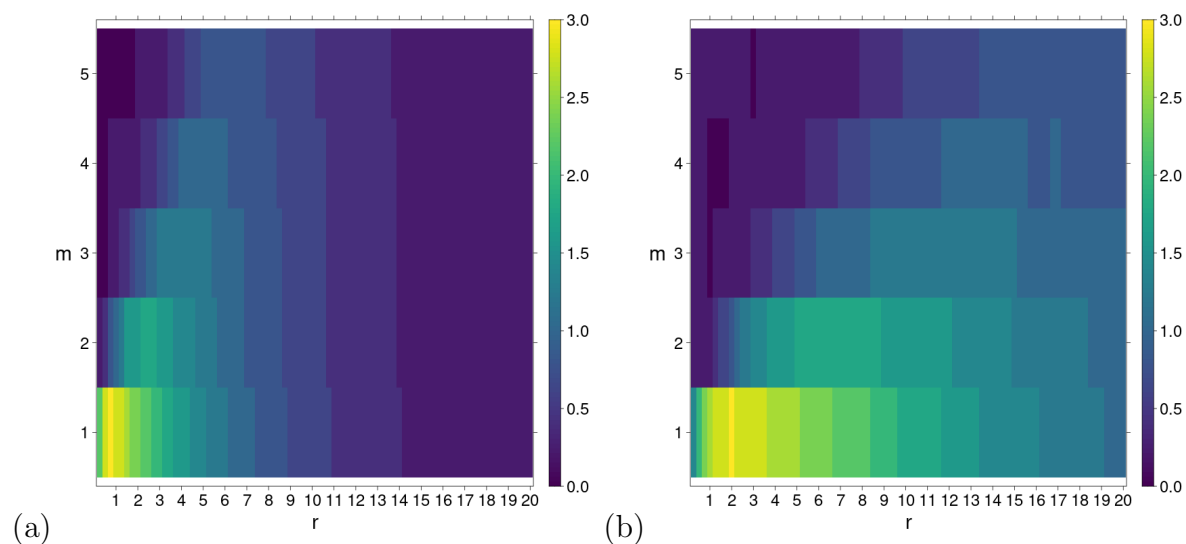


**Figure 3.** Simulated data demonstrating how  $ApEn$  varies with  $m$  and  $r$  for (a) normal phase image and (b) a phase image for an MI

### 3.2. Final selection of tolerance parameter ( $r$ )

To determine the optimal value of  $r$ ,  $ApEn$  was calculated and plotted for simulated normal and MI phase patterns using  $m=2$ , and a range of  $r$ , as shown in Figure 4. These graphs demonstrate that  $ApEn$  increases from zero, peaks, then decreases gradually to zero again as  $r$  is increased. The maximum discrimination between the two groups that are plotted is  $r = 1.75$ . Importantly, there is a value of  $r$  where the  $ApEn$  calculated from both phase images is equal, emphasising the need for using an appropriate value of  $r$ . If a value of  $r$  is selected that is below the 'flip point', then a higher  $ApEn$  is normal, whilst if a larger value of  $r$  is used, a higher  $ApEn$  would suggest that the phase is abnormal. These results are consistent with the literature, which suggests that  $ApEn$  can flip when the input values are changed [19].

Plotting the results of the normal, MI and LBBB patient groups (Figure 5) shows that the maximum discrimination for this group is at  $r=1$  and the point where all three patient groups had equal  $ApEn$  was at  $r = 2.75$ . The most critical point when considering the selection of input parameters is avoiding the area where abnormal and normal are equal. This point on the graph will vary, depending on how 'abnormal' the phase is. At this point, work was continued with two values of  $r$ ,  $r = 1$  and  $r = 7$ . These values were chosen because they provided adequate separation between normal and abnormal phase but were not close to the 'flip' point.

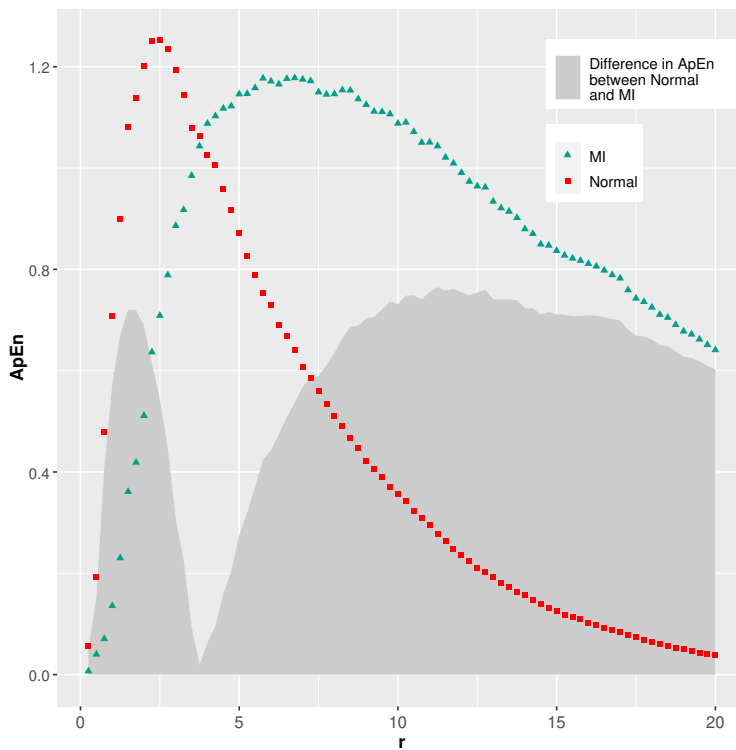
### 3.3. Effect of data length

$ApEn$  does not vary significantly as the number of pixels is increased when  $r=7$ , as demonstrated in Figure 6. However, for  $ApEn[r=1]$  the value of  $ApEn$  increases when the LV size increases, meaning that  $ApEn[r=1]$  is not appropriate for this data. A possible explanation for this might be that when the chosen value of  $r$  is low, the bias effect due to the self-matches has a more significant impact. Unlike time-series data like an ECG or gait, it is impossible to control the length of the data series for RNVG phase data. The length of the data will depend on the size of the LV, which will be patient dependent so  $ApEn$  should be consistent across the clinical range. For this reason, a final value of  $r = 7$  was selected for  $ApEn$ .

### 3.4. Data order



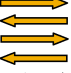

Table 1 shows the mean  $ApEn(m=2,r=7)$  for each group and the  $AUC$  value with 95%  $CI$  for phase data read in different directions. As expected, there is a small difference in  $ApEn$  for different data orders. However, the results indicate that the data order does not affect the ability of  $ApEn$  to discriminate between normal and abnormal phase. The  $ROC$  curves for each data order are shown in Figure 7.  $AUC$  values ranging from 0.715 to 0.746 were achieved for the four different data orders.  $ApEn$  is lower for directions (c) and (d), this is likely because for each group of  $m$  the pixels are next to each other, resulting in more matches and lower  $ApEn$ . While the data order did not significantly





**Figure 4.** Simulated data which represents a phase image for normal LV contraction (in red) and a large MI (in blue), demonstrating how  $ApEn$  varies with increasing tolerance  $r$ , where sequence length  $m = 2$ . The shaded area represents the difference in  $ApEn$  between the normal and MI phase images.

**Table 1.** Summary of statistics for data order

Data Order	Normal Group <i>Mean <math>\pm</math> SD</i>	MI Group <i>Mean <math>\pm</math> SD</i>	<i>AUC</i>	<i>95% CI</i>
(a) 	$0.460 \pm 0.138$	$0.556 \pm 0.116$	0.72	0.66-0.77
(b) 	$0.457 \pm 0.129$	$0.566 \pm 0.119$	0.75	0.67-0.77
(c) 	$0.418 \pm 0.135$	$0.520 \pm 0.118$	0.73	0.65-0.76
(d) 	$0.414 \pm 0.133$	$0.524 \pm 0.124$	0.74	0.67-0.77

affect the  $AUC$  values, order (c) and (d) are preferred because the pixels in each group of  $m$  are adjacent.

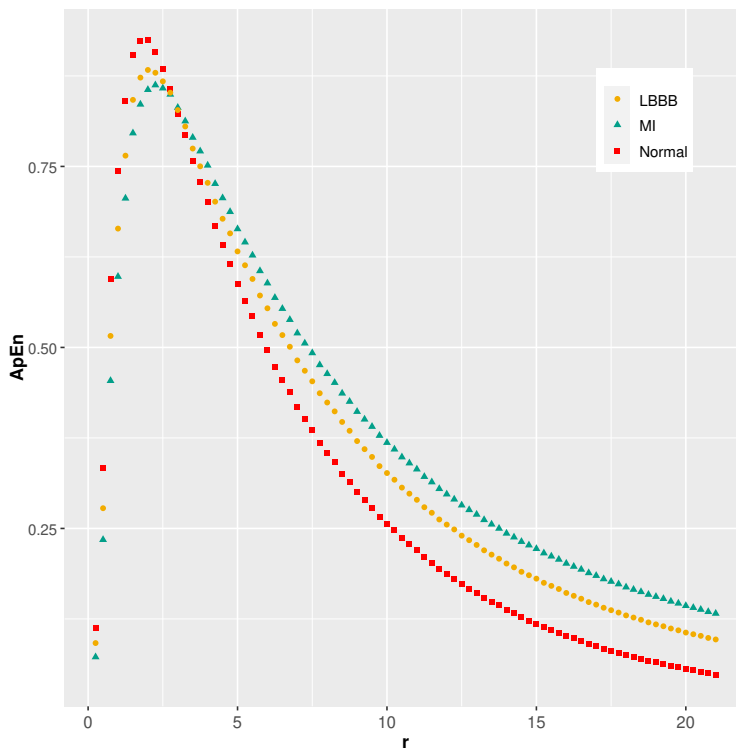


**Figure 5.** Average  $ApEn$  for normal (red), MI (green) and LBBB (yellow) patient groups using varying values of tolerance  $r$ , where  $m=2$ .

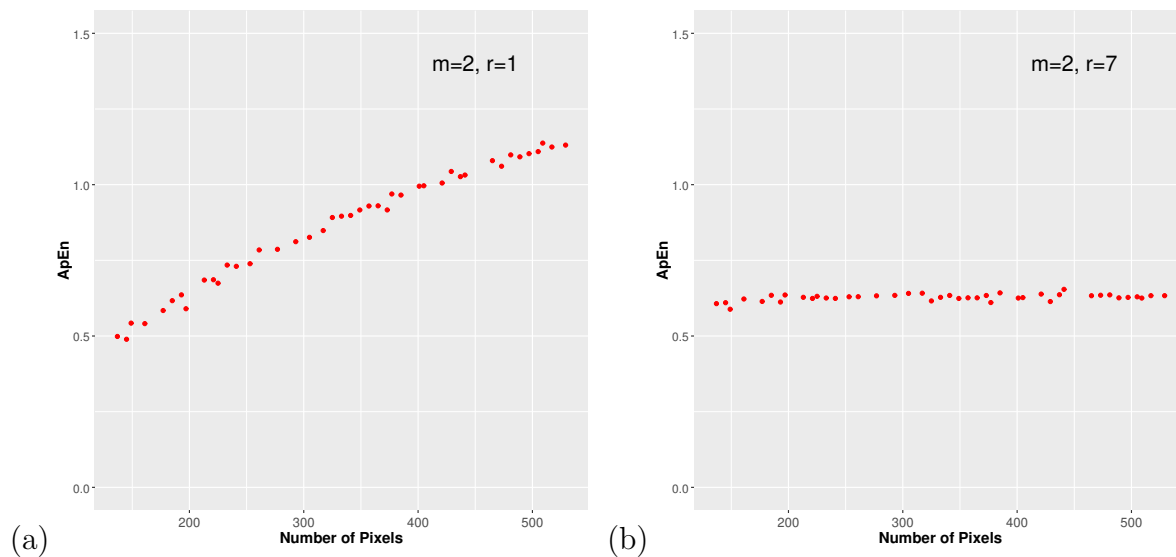


**Figure 6.** Variation of  $ApEn$  with LV size for (a)  $m=2$ ,  $r=1$  (b)  $m=2$ ,  $r=7$ , demonstrating a lack of consistency for  $r=1$  with increasing ventricle size for simulated data.

#### 4. Conclusions

Appropriate input parameters for  $ApEn$  applied to RNVG phase images have been established using both simulated and patient data. The results justify the input

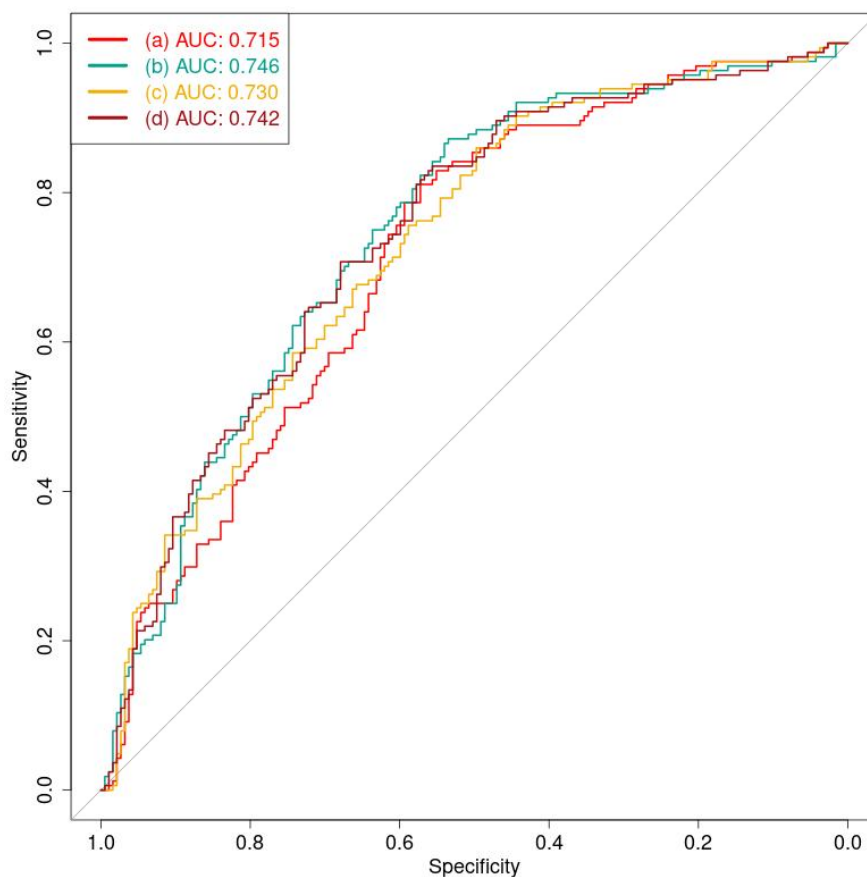


**Figure 7.** ROC analysis for each data order, comparing the difference between normal and MI groups

parameters selected and demonstrate that they are appropriate for application to RNVG phase images. This work highlights the importance of optimising input parameters when using novel indices, such as  $ApEn$ , to characterise clinical images. Standardisation is crucial, and although this work investigates  $ApEn$  for a specific case, it demonstrates the importance of optimisation and standardisation. Further work is required to establish the reproducibility and normal range for clinical use.

**References**

- [1] M. S. J. Sutton, M. A. Pfeffer, L. Moye, T. Plappert, J. L. Rouleau, G. Lamas, J. Rouleau, J. O. Parker, M. O. Arnold, B. Sussex, *et al.*, “Cardiovascular death and left ventricular remodeling two years after myocardial infarction: baseline predictors and impact of long-term use of captopril: information from the survival and ventricular enlargement (save) trial,” *Circulation*, vol. 96, no. 10, pp. 3294–3299, 1997.
- [2] M. M. McDermott, J. Feinglass, P. I. Lee, S. Mehta, B. Schmitt, F. Lefevre, and M. Gheorghiade, “Systolic function, readmission rates, and survival among consecutively hospitalized patients with congestive heart failure,” *American heart journal*, vol. 134, no. 4, pp. 728–736, 1997.
- [3] S. D. Solomon, N. Anavekar, H. Skali, J. J. McMurray, K. Swedberg, S. Yusuf, C. B. Granger, E. L. Michelson, D. Wang, S. Pocock, *et al.*, “Influence of ejection fraction on cardiovascular outcomes in a broad spectrum of heart failure patients,” *Circulation*, vol. 112, no. 24, pp. 3738–3744, 2005.
- [4] J. Cullen, A. Saleem, R. Swindell, P. Burt, and C. Moore, “Measurement of cardiac synchrony using approximate entropy applied to nuclear medicine scans,” *Biomedical Signal Processing and Control*, vol. 5, pp. 32–36, 1 2010.
- [5] K. A. Jones, A. D. Small, S. Ray, D. J. Hamilton, J. Robinson, N. E. R. Goodfield, and C. A. Paterson, “Radionuclide ventriculography phase analysis for risk stratification of patients undergoing cardiotoxic cancer therapy,” *Journal of Nuclear Cardiology*, <https://doi.org/10.1007/s12350-020-02277-z> 2020.
- [6] E. H. Botvinick, M. B. Fraiss, D. W. Shosa, M. A. O’Connell, J. A. Pacheco-Alvarez, M. Scheinman, R. S. Hattner, F. Morady, and D. B. Faulkner, “An accurate means of detecting and characterizing abnormal patterns of ventricular activation by phase image analysis,” *The American Journal of Cardiology*, vol. 50, pp. 289–298, 1982.
- [7] M. Fraiss, E. H. Botvinick, D. W. Shosa, W. J. O’Connell, M. M. Scheinman, R. S. Hattner, and F. Morady, “Phase image characterization of ventricular contraction in left and right bundle branch block,” *The American Journal of Cardiology*, vol. 50, pp. 95–105, 1982.
- [8] S. M. Pincus, I. M. Gladstone, and R. A. Ehrenkranz, “A regularity statistic for medical data analysis,” *Journal of clinical monitoring*, pp. 335–345, 1991.
- [9] G. S. Dawes, M. Moulden, O. Sheil, and C. W. Redman, “Approximate entropy, a statistic of regularity, applied to fetal heart rate data before and during labor,” *Obstetrics and gynecology*, vol. 80, pp. 763–768, November 1992.
- [10] M. P. Tulppo, T. H. Makikallio, T. E. Takala, T. Seppanen, and H. V. Huikuri, “Quantitative beat-to-beat analysis of heart rate dynamics during exercise,” *American Journal of Physiology-Heart and Circulatory Physiology*, vol. 271, no. 1, pp. H244–H252, 1996.

- [11] A. D. Georgoulis, C. Moraiti, S. Ristanis, and N. Stergiou, “A novel approach to measure variability in the anterior cruciate ligament deficient knee during walking: The use of the approximate entropy in orthopaedics,” *Journal of Clinical Monitoring and Computing*, vol. 20, no. 1, pp. 11–18, 2006.
- [12] A. H. Khandoker, M. Palaniswami, and R. K. Begg, “A comparative study on approximate entropy measure and poincaré plot indexes of minimum foot clearance variability in the elderly during walking,” *Neuroeng Rehabil*, vol. 5, p. 4, 2008.
- [13] S. M. Pincus and E. K. Kalman, “Irregularity, volatility, risk, and financial market time series,” *Proceedings of the National Academy of Sciences*, vol. 101(38), pp. 13709–13714, 2004.
- [14] S. M. Pincus and A. L. Goldberger, “Physiological time-series analysis: what does regularity quantify?,” *The American Journal of Physiology*, vol. 266 (4), pp. 1643–1656, 1994.
- [15] R. A. McKinley, L. K. McIntire, R. Schmidt, D. W. Repperger, and J. A. Caldwell, “Evaluation of eye metrics as a detector of fatigue,” *Human Factors*, vol. 53 (4), pp. 403–414, 2011.
- [16] K. Yun, “Decreased cortical complexity in methamphetamine abusers,” *Psychiatry Research: Neuroimaging*, vol. 201(3), pp. 226–32, 2012.
- [17] J. M. Yentes, N. Hunt, K. K. Schmid, J. P. Kaipust, D. McGrath, and N. Stergiou, “The appropriate use of approximate entropy and sample entropy with short data sets,” *Annals of Biomedical Engineering*, vol. 42, pp. 349–65, 2012.
- [18] A. Delgado-Bonal and A. Marshak, “Approximate entropy and sample entropy: A comprehensive tutorial,” *Entropy*, vol. 21 6, p. 541, 2019.
- [19] J. M. Yentes, W. Denton, J. McCamley, P. Raffalt, and K. K. Schmid, “Effect of parameter selection on entropy calculation for long walking trials,” *Gait Posture*, vol. 60, pp. 128–134, 2018.
- [20] L. Montesinos, R. Castaldo, and L. Pecchia, “On the use of approximate entropy and sample entropy with centre of pressure time-series,” *J NeuroEngineering Rehabil*, vol. 15, 2018.
- [21] R Core Team, *R: A Language and Environment for Statistical Computing*. R Foundation for Statistical Computing, Vienna, Austria, 2018.
- [22] S. M. Pincus, “Approximate entropy as a measure of system complexity,” *Mathematics*, vol. 88, pp. 2297–2301, 1991.